AIAA JOURNAL
Vol. 34, No. 2, February 1996

Computation of Turbulent Axisymmetric and Nonaxisymmetric Jet Flows Using the K–ε Model

Andrew T. Thies* and Christopher K. W. Tam†
Florida State University, Tallahassee, Florida 32306-3027

It is known that the standard K–ε model does not provide an accurate prediction of the mean flow of turbulent jets. This is so even when the Pope and Sarkar correction terms are included. It is suggested that the K–ε model, together with the Pope and Sarkar terms for nonplanar and high convective Mach number flow corrections, does contain the essential ingredients of turbulence physics for adequate jet mean flow prediction. The problem lies in the standard coefficients that were calibrated by using boundary-layer and low Mach number plane mixing layer data. By replacing these coefficients by a new set of empirical coefficients, it is demonstrated that the model can offer good predictions of axisymmetric, rectangular, and elliptic jet mean flows over the Mach number range of 0.4–2.0 and jet total temperature to ambient temperature ratio of 1.0–4.0. The present result conveys the message that it is possible that there is no universally applicable turbulence model. The reason is that although the characteristics and dynamics of fine-scale turbulence may be the same for all turbulent flows, the large turbulence structures, having dimensions comparable to the local length scale of the flow, are significantly influenced by local boundary conditions and geometry. Thus overall turbulence dynamics are somewhat problem type dependent.

I. Introduction

THIS paper is motivated by the authors' interest in supersonic jet noise prediction. It is known that both the large turbulence structures and the fine-scale turbulence of a high-speed jet are important sources of noise. The large turbulence structures radiate sound in the form of Mach waves. They are the dominant source of turbulent mixing noise of jets when the jet velocity is highly supersonic relative to the ambient sound speed. The Mach wave radiation can be predicted by a stochastic instability wave model theory.[1] One requirement of this theory is that the mean velocity and density profiles of the jet must be known. Thus, the calculation of the jet mean flow distribution is a needed first step of high-speed jet noise prediction. As the jet speed decreases, the contribution of noise from the fine-scale turbulence becomes increasingly important. The intensity of the radiated noise is directly related to the intensity of the fine-scale turbulence. A first-order estimate of the turbulence intensity can be obtained via the K–ε turbulence model equations. The use of the K–ε model to calculate the mean flow and the length or time scales and intensity of turbulence of a jet is, therefore, an attractive way of obtaining valuable flow information for noise prediction. This approach has recently been adopted by Khavaran et al.[2] and Bailly et al.[3]

The K–ε turbulence model has proven, over the years, to be a useful engineering approach for the prediction of the mean velocity profiles of turbulent flows. Much has been written about the model. For a review on this subject and the broader subject of turbulence modeling, the readers are referred to a recent review article by Speziale.[4]

In the development of the standard K–ε model during the early seventies,[5–8] there was a general belief that the nature and characteristics of turbulence were universally the same. As a result, a good turbulence model was expected to be applicable to turbulent boundary layers as well as to turbulent free shear flows. Most of the early applications of the standard K–ε model were for turbulent boundary-layer and plane shear layer flows. Because of this, the unknown constants of the model were determined by minimizing the difference between the calculated results based on the model and the measured velocity profiles of these flows. These constants have been well accepted and widely used to this day.[4]

Received Dec. 12, 1994; revision received July 14, 1995; accepted for publication Aug. 7, 1995. Copyright © 1995 by A. T. Thies and C. K. W. Tam. Published by the American Institute of Aeronautics and Astronautics, Inc., with permission.

*Graduate Student, Department of Mathematics. Student Member AIAA.
†Professor, Department of Mathematics. Associate Fellow AIAA.

It became known in the late seventies that the standard K–ε model was not capable of predicting accurately the mean velocity profiles of turbulent axisymmetric jets.[9] In the intervening years, various investigators proposed different schemes to correct this and other deficiencies. One popular approach is to add correction terms. This practice continues to the present time.[10,11] Some correction terms are purely empirical. We may regard them as a form of curvefitting. Others, based on geometrical and physical reasonings, are quite well justified. For example, Pope[9] argued that turbulent axisymmetric mixing was different from two-dimensional mixing layers. One way to see Pope's argument is to recognize that turbulent motion in jet flows ranges from large to very small scales. Although the small-scale motion might be sufficiently universal and would not be affected by the geometry of the flow, the large-scale motion, having dimensions of the same order as the flowfield, is inevitably influenced by the flow geometry. For this reason, the turbulence of an axisymmetric jet would not be the same as that in a plane jet. Pope quantified his argument by appealing to the notion of vortex stretching. He formulated a correction term according to this premise. By design, Pope's correction term becomes identically equal to zero for incompressible plane flows. For three-dimensional flows, it increases the dissipation rate and hence reduces the turbulence intensity. This results in an automatic reduction in the spreading rate of the mean flow. To specify the value of the unknown constant of his correction term, Pope used turbulent axisymmetric jet mean velocity data available to him at that time. It is worthwhile to point out that the measurements used were from nearly incompressible jets.

For high-speed mixing layers and jets, it has been found experimentally that the efficiency of the mixing process is greatly reduced.[12–14] Papamoschou and Roshko[14] demonstrated that the reduction in the growth rate of high-speed mixing layers correlated well with the reduction in the growth rate of the instability waves of the flow, when considered as a function of convective Mach number. This finding should not be too surprising since the instabilities of the flow are the primary mechanisms that transfer energy from the mean flow to the large turbulence structures. The large turbulence structures, in turn, are the driving force of the turbulent mixing process. Thus, the growth rate of the turbulent shear layer must directly tie in to the growth rate of the flow instabilities. Sarkar et al.[15] and Sarkar and Lakshmanan,[16] motivated by these experimental observations, proposed the addition of a new correction to the K–ε model to account for this effect. He developed a correction model based on a somewhat different argument. The form of the correction model was found by an asymptotic analysis of the compressible Navier–Stokes equations.[15] The unknown coefficient was

calibrated by direct numerical simulations of compressible isotropic turbulence. Although the Sarkar model was derived on a vastly different physical basis, yet it has exactly the correct form to render the observed high convective Mach number effects. Calculated results consistently show improved predictions when the Sarkar correction is included in the K–ε model.

Our interest is to find a turbulence model that would allow us to obtain reasonably accurate jet mean flow prediction over the jet Mach number range of 0.4–2.0 and temperature ratio from 1.0 (cold jet) to 4.0. This parameter range includes the operating conditions of most commercial aircraft jet engines. Naturally, we tried to use the K–ε model together with the Pope and Sarkar corrections. Much to our disappointment, we found quickly that our objective could not be realized. This is so even if we confine ourselves to axisymmetric jets alone. It turns out that in the literature others have documented a similar difficulty.[10,11]

We have since performed a careful examination of the basis of the K–ε model and the Pope and Sarkar corrections. We are convinced that the combined model does contain the essential physics of turbulence needed for jet mean flow prediction. We suspect the problem is, perhaps, not so much with the model but with the original belief that the model should have universal application. Recall that the coefficients of the standard K–ε model were adopted as universal constants, although they were calibrated by using only turbulent boundary-layer and plane mixing layer data. It is, therefore, possible that these coefficients are not appropriate for jet flow prediction.

The purpose of this paper is to demonstrate that if the coefficients of the standard K–ε model and the original coefficients of the Pope and Sarkar correction terms are replaced by a new set of values, found empirically, the calculated jet mean velocity profiles agree well with measurements over the preceding specified parameter range. These new coefficients and detailed comparisons between calculated jet mean velocity profiles and measurements are reported in Sec. IV of this paper. The K–ε model, with the Pope and Sarkar correction terms and the new coefficients, has also been applied to the prediction of the mean flows of nonaxisymmetric jets. Specifically, both rectangular and elliptic jets have been considered. Good agreements with experimental measurements are found (however, not as good as for axisymmetric jets). It is believed that the calculated results are good enough as a starting point for jet noise prediction.

II. K–ε Model Equations and Correction Terms

Dimensionless variables with ρ_j, p_j, T_j, u_j, and D, the nozzle exit density, pressure, temperature, velocity, and diameter, as the density, pressure, temperature, velocity, and length scales will be used. The turbulence quantities K and ε will be nondimensionalized by u_j^2 and by u_j^3/D, respectively. The Favre-averaged equations of motion, including the K–ε model as well as the Pope and Sarkar correction terms in nondimensional form, are

$$\frac{\partial u_k}{\partial x_k} - \frac{u_k}{T}\frac{\partial T}{\partial x_k} = -\frac{u_k}{p}\frac{\partial p}{\partial x_k} \tag{1}$$

$$\rho u_k \frac{\partial u_i}{\partial x_k} = -\frac{1}{\gamma M_j^2}\frac{\partial p}{\partial x_i} - \frac{\partial(\rho\tau_{ik})}{\partial x_k} \tag{2}$$

$$\gamma\rho u_k\frac{\partial T}{\partial x_k} = (\gamma-1)u_k\frac{\partial p}{\partial x_k} + \gamma(\gamma-1)M_j^2\rho\varepsilon + \frac{1}{\sigma_T}\frac{\partial}{\partial x_k}\left(\frac{\rho}{Re_t}\frac{\partial T}{\partial x_k}\right) \tag{3}$$

$$\rho u_k\frac{\partial K}{\partial x_k} = -\rho\tau_{ik}\frac{\partial u_i}{\partial x_k} - \rho\varepsilon + \frac{1}{\sigma_K}\frac{\partial}{\partial x_k}\left(\frac{\rho}{Re_t}\frac{\partial K}{\partial x_k}\right) \tag{4}$$

$$\rho u_k\frac{\partial \varepsilon_s}{\partial x_k} = -C_{\varepsilon 1}\frac{\varepsilon_s}{K}\rho\tau_{ik}^s\frac{\partial u_i}{\partial x_k} - (C_{\varepsilon 2} - C_{\varepsilon 3}\chi)\rho\frac{\varepsilon_s^2}{K} + \frac{1}{\sigma_\varepsilon}\frac{\partial}{\partial x_k}\left(\frac{\rho}{Re_t^s}\frac{\partial \varepsilon_s}{\partial x_k}\right) \tag{5}$$

$$p = \rho T \tag{6}$$

where

$$1/Re_t = C_\mu K^2/\varepsilon \tag{7}$$

$$1/Re_t^s = C_\mu K^2/\varepsilon_s \tag{8}$$

$$\varepsilon = \varepsilon_s\left(1 + \alpha_1 M_t^2\right) \tag{9}$$

$$M_t^2 = (2K/T)M_j^2 \tag{10}$$

$$\tau_{ik} = \frac{2}{3}K\delta_{ik} - \frac{1}{Re_t}\left(\frac{\partial u_i}{\partial x_k} + \frac{\partial u_k}{\partial x_i} - \frac{2}{3}\frac{\partial u_j}{\partial x_j}\delta_{ik}\right) \tag{11}$$

$$\tau_{ik}^s = \frac{2}{3}K\delta_{ik} - \frac{1}{Re_t^s}\left(\frac{\partial u_i}{\partial x_k} + \frac{\partial u_k}{\partial x_i} - \frac{2}{3}\frac{\partial u_j}{\partial x_j}\delta_{ik}\right) \tag{12}$$

$$\chi = \omega_{ij}\omega_{jk}s_{ki}$$

$$\omega_{ij} = \frac{1}{2}\frac{K}{\varepsilon_s}\left(\frac{\partial u_i}{\partial x_j} - \frac{\partial u_j}{\partial x_i}\right) \tag{13}$$

$$s_{ij} = \frac{1}{2}\frac{K}{\varepsilon_s}\left(\frac{\partial u_i}{\partial x_j} + \frac{\partial u_j}{\partial x_i}\right) \tag{14}$$

where M_j is the jet Mach number and γ is the ratio of specific heats.

Equation (1) is the continuity equation in which ρ has been eliminated in favor of p and T by the equation of state. The preceding system of equations contains eight empirical constants, six of which, namely, C_μ, $C_{\varepsilon 1}$, $C_{\varepsilon 2}$, σ_T, σ_K, and σ_ε, are from the K–ε model. The constant $C_{\varepsilon 3}$ is from the Pope correction term and σ_1 is from the Sarkar correction term. The choice of the values of these constants is a critical issue in this work and will be discussed later.

For jet flows, Eqs. (1–5) may be parabolized to allow easy numerical computation of their solution. An in-depth discussion of the appropriateness of parabolizing these equations can be found in Ref. 17 and the references therein. In this work, the following steps are taken to achieve parabolization: 1) the $\partial p/\partial x$ term in the axial momentum equation (the x axis coincides with the centerline of the jet) is neglected (boundary-layer approximation); 2) the pressure gradient terms in the energy equation are neglected (boundary-layer approximation); 3) outside the jet, it is assumed that there is a uniform mean flow equal to 2% or less of the jet exit velocity (parabolizing approximation); 4) all eddy viscosity terms involving x derivatives are neglected (small compared with derivatives in the transverse direction); and 5) the diffusion terms of the energy, turbulence energy, and the ε_s equations involving gradients in the axial direction are neglected (small compared with diffusion in the transverse direction).

Upon parabolization, Eqs. (1–5) may be cast in the form

$$\frac{\partial \boldsymbol{u}}{\partial x} = \boldsymbol{F} \tag{15}$$

where

$$\boldsymbol{u} = [p, u, v, w, T, K, \varepsilon_s]^T$$

and where T = transpose. In Eq. (15), u, v, and w are the velocity components in the x, y, and z directions. It is worthwhile to note that the right side $\boldsymbol{F}$ of Eq. (15) no longer contains any x derivatives. Thus, starting from a set of initial conditions at the nozzle exit, an accurate solution can be found by using a numerical marching scheme in the x direction. In the case of axisymmetric jets, a simpler system of equations may be used. This is accomplished by applying the boundary-layer approximation to the radial momentum equation yielding p = const as the solution. Only the variables u, T, K, and ε_s need to be calculated by the marching scheme. The remaining unknown, the radial velocity component v, is determined by solving the continuity equation implicitly after each marching step has been completed. Extensive investigations indicate that both the general marching method using Eq. (15) and the simplified method for axisymmetric jets give essentially identical numerical results.[18]

The two independent methods of solution provide assurance that the numerical results are accurate.

A number of terms in Eqs. (5–14) have turbulence quantities ε, ε_s, or K in the denominator. Since these quantities are essentially zero outside the jet, the terms may become numerically unbounded as a result of division by zero. To avoid such numerical problems, in this work, the problematic denominators are replaced by $(\varepsilon+\varepsilon_0)$, $(\varepsilon_s+\varepsilon_0)$, and $(K+K_0)$, respectively. For example, Re_t^{-1} in Eq. (7) is replaced by

$$1/Re_t = C_\mu K^2/[\varepsilon+\varepsilon_0]$$

where ε_0 and K_0 are small positive numbers. Numerical experiments indicate that these modifications have negligible influence on the computed solution. Their role is simply to prevent the computer from executing division by zero.

III. Computation Scheme and Initial and Boundary Conditions

To facilitate marching in the x direction, the y–z plane is divided into a rectangular mesh. A finer mesh is used in the mixing layer region of the jet. A detailed layout of the mesh is given in Ref. 18. Transverse derivatives in the y and z directions on the right side of Eq. (15) are approximated by seven-point finite differences according to the dispersion-relation-preserving (DRP) scheme.[19] For example, with subscripts l and m denoting the mesh points in the y and z directions and superscript n indicating the number of steps in the x direction, the transverse derivatives are approximated by

$$\frac{\partial f}{\partial y} \simeq \frac{1}{\Delta y}\sum_{j=-3}^{3} a_j f_{l+j,m}^{(n)}$$
$$\frac{\partial f}{\partial z} \simeq \frac{1}{\Delta z}\sum_{j=-3}^{3} a_j f_{l,m+j}^{(n)} \tag{16}$$

where the coefficients a_j can be found in Ref. 20 and Δy and Δz are the mesh sizes. The axial marching procedure utilizes the third-order Adams–Bashforth method. In discretized form Eq. (15) becomes

$$\boldsymbol{u}_{l,m}^{(n+1)} = \boldsymbol{u}_{l,m}^{(n)} + \Delta x \sum_{j=0}^{3} b_j \boldsymbol{F}_{l,m}^{(n-j)} \tag{17}$$

where Δx is the step size.

Spurious numerical waves are inevitably generated by the initial conditions and at the mesh interface where there is a change in mesh size. To eliminate these unwanted waves, artificial selective damping terms[20,21] are added to the computation scheme. Detailed analysis of the numerical stability boundary of the marching scheme has been carried out.[18] The stability requirements are most stringent in the shear layer and at the outside edge of the jet flow. They dictate the step size Δx used in the computation.

A nonuniform grid in the y–z plane with a larger concentration of grid points in the mixing layer of the jet is used in the computation. Close to the nozzle exit, a very fine grid is employed to resolve the thin mixing layer. As the computation proceeds downstream, half of the grid lines are removed when the computation reaches the location where the mixing layer thickness is twice that at the nozzle exit. This coarsening of the grid does not compromise the spatial resolution of the computation. But it allows the marching step size Δx to increase. This greatly reduces the overall computation time. This grid adjustment process is repeated several times during the course of a complete run over the entire jet. To ensure accuracy, the computed results have been selectively checked by occasionally repeating a run using deliberately smaller grid and marching steps. It has been found that as long as the Δx used is within numerical stability limit, the computed jet velocity profiles remain essentially unchanged.

Initial jet flow data at the nozzle exit were often not measured in most experiments reported in the literature. In the absence of such information, the quantities v, w, K, and ε_s are simply initialized to zero. The term p is set to unity. The remaining variables are chosen to have the form

$$u(0,y,z) = u_\infty + (1-u_\infty) f(y,z) \tag{18}$$

$$T(0,y,z) = T_\infty + (1-T_\infty) f(y,z) \tag{19}$$

where u_∞ and T_∞ are the freestream velocity and temperature outside the jet. The function f is taken to be

Axisymmetric jet:

$$f(r) = \begin{cases} 1, & r \le h \\ \exp[-\ell n 2((r-h)/b)^2], & r > h \end{cases} \tag{20}$$

Rectangular jet:

$$f(x,y) = \begin{cases} 1, & |y| \le h_y, \quad |z| \le h_z \\ \exp\left[-\ell n 2\left(\dfrac{|y|-h_y}{b_y}\right)^2\right], & |y| > h_y, \quad |z| \le h_z \\ \exp\left[-\ell n 2\left(\dfrac{|z|-h_z}{b_z}\right)^2\right], & |y| \le h_y, \quad |z| > h_z \\ \exp\left\{-\ell n 2\left[\left(\dfrac{|y|-h_y}{b_y}\right)^2 + \left(\dfrac{|z|-h_z}{b_z}\right)^2\right]\right\}, & |y| > h_y, \quad |z| > h_z \end{cases} \tag{21}$$

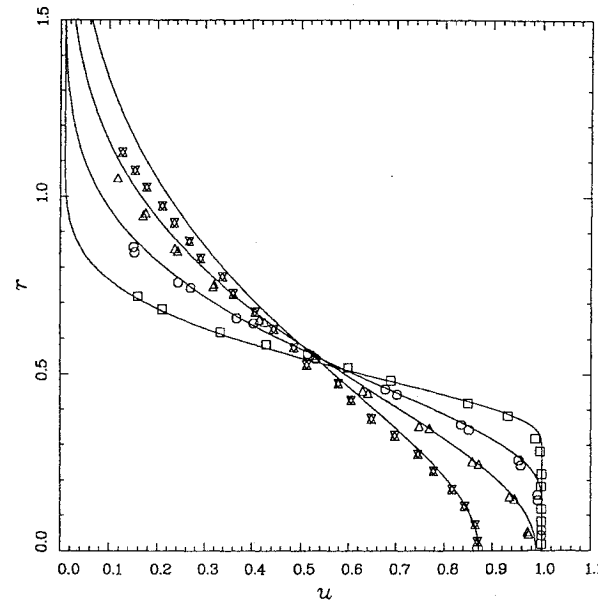

Fig. 1 Comparisons of computed and measured axial velocity profiles for Schreck et al.'s[22] cold, Mach 0.4, axisymmetric jet: □, x = 2.0; ○, x = 4.0; △, x = 6.0; and ⊠, x = 8.0.

Table 1 Axisymmetric jets

Source of data	M_j	T_r/T_a	Data type	Figure
Schreck et al.[22]	0.4	1.0	Velocity profiles	1
Schreck et al.[22]	0.6	1.0	Velocity profiles	2
Schreck et al.[22]	0.9	1.0	Velocity profiles	3
Laurence[23]	0.7	1.0	Velocity profiles	4
Maestrello and McDaid[24]	0.66	1.0	Centerline velocity	5
Laurence[23]	0.7	1.0	Centerline velocity	5
Seiner[25]	1.5	1.12	Centerline velocity and Mach number	6
Seiner et al.[26]	2.0	1.0	Centerline Mach number and jet half-width	7
Seiner et al.[27]	2.0	1.12	Centerline velocity and jet half-width	8
Seiner et al.[27]	2.0	2.72	Centerline velocity and jet half-width	9
Seiner et al.[27]	2.0	4.0	Centerline velocity and jet half-width	10
Eggers[28]	2.22	1.0	Centerline velocity and jet half-width	11

Table 2 Rectangular and elliptic jets

Source of data	M_j	T_r/T_a	Jet configuration	Figure
Schreck et al.[22]	0.4	1.0	Aspect ratio 2 rectangular jet	12
Schreck et al.[22]	0.6	1.0	Aspect ratio 2 rectangular jet	13
Schreck et al.[22]	0.4	1.0	Aspect ratio 3 rectangular jet	14
Schreck et al.[22]	0.6	1.0	Aspect ratio 3 rectangular jet	15
Schreck et al.[22]	0.9	1.0	Aspect ratio 3 rectangular jet	16
Seiner[25]	1.5	1.12	Aspect ratio 2 elliptic jet	17

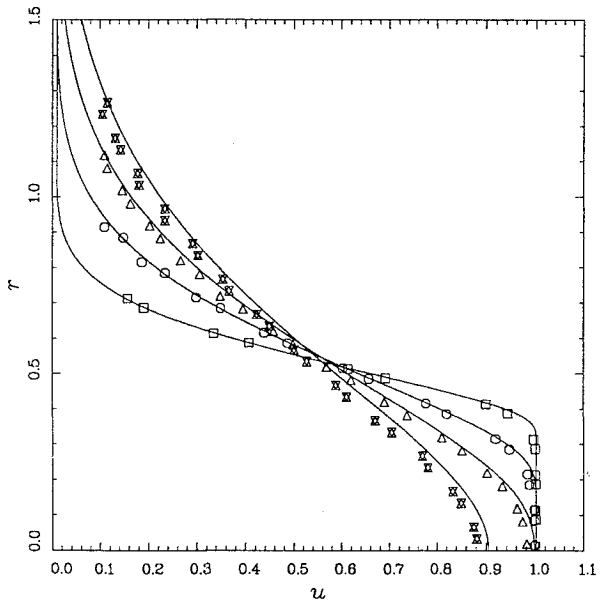

Fig. 2 Comparisons of computed and measured axial velocity profiles for Schreck et al.'s[22] cold, Mach 0.6, axisymmetric jet: □, x = 2.0; ○, x = 4.0; △, x = 6.0; and ⊠, x = 8.0.

Elliptic jet: An initial velocity and temperature distribution similar to the preceding but expressed in parametric form is used (see Ref. 18 for details).

In the computation, the core size h(h_y and h_z in the case of rectangular jet) and shear layer half-width b (or b_y and b_z) are chosen such that the solution matches the first measured data at some downstream location. It is important that the solution has reached

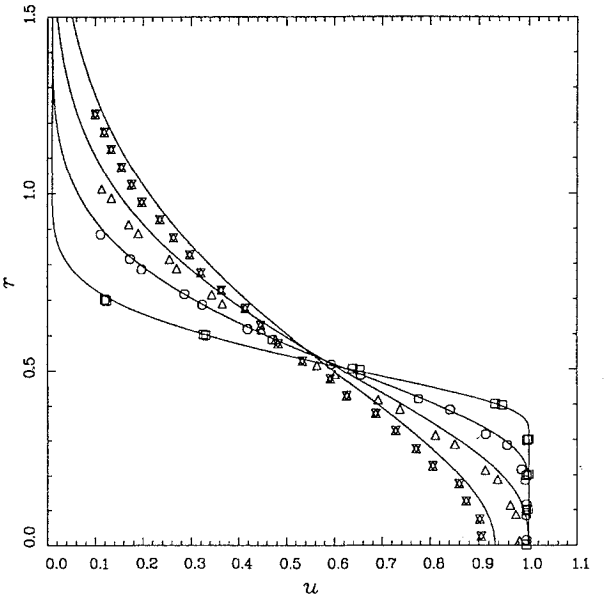

Fig. 3 Comparisons of computed and measured axial velocity profiles for Schreck et al.'s[22] cold, Mach 0.9, axisymmetric jet: □, x = 2.0; ○, x = 4.0; △, x = 6.0; and ⊠, x = 8.0.

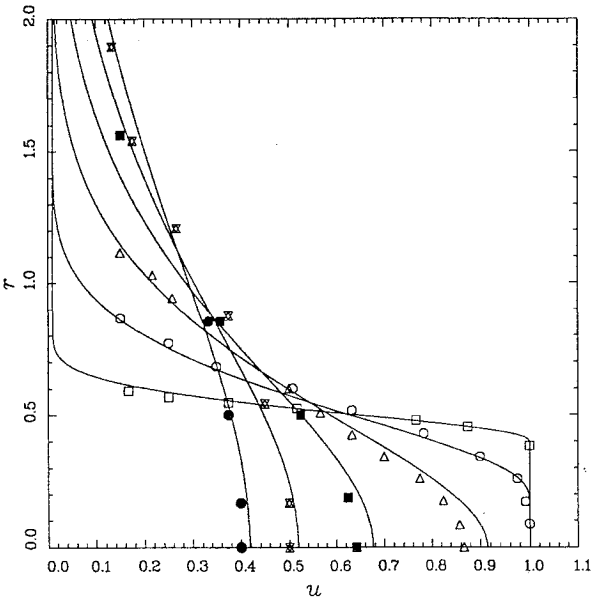

Fig. 4 Comparisons of computed and measured axial velocity profiles for Laurence's[23] cold, Mach 0.7, axisymmetric jet: □, x = 1.1; ○, x = 4.0; △, x = 8.0; ■, x = 12.0; ⊠, x = 16.0; and ●, x = 20.0.

quasi-equilibrium before comparison with the data is first made. Experience shows that nearly the same quasi-equilibrium solution is obtainable from a range of initial conditions. Thus the computed solution is not unduly sensitivity to initial conditions.

At some distance outside the jet, the flow is approximately axisymmetric. In this region the flow is given by the linearized form of Eq. (15). With $u = u_\infty$ (the uniform flow outside the jet), $T = T_\infty$, $p = 1 + p'$, and V = radial velocity, the continuity and radial momentum equations in cylindrical coordinates reduce to

$$u_\infty \frac{\partial(p'r)}{\partial x} = -\frac{\partial}{\partial r}(Vr) \tag{22}$$

$$u_\infty \frac{\partial(Vr)}{\partial x} = -\frac{T_\infty}{\gamma M_j^2}\left[\frac{\partial(p'r)}{\partial r} - \frac{p'r}{r}\right] \tag{23}$$

To find the correct boundary condition for Eq. (15) in this region, we will first seek a solution of these equations for small u_∞($u_\infty \ll 1$). The left and right sides of Eq. (22) are balanced if

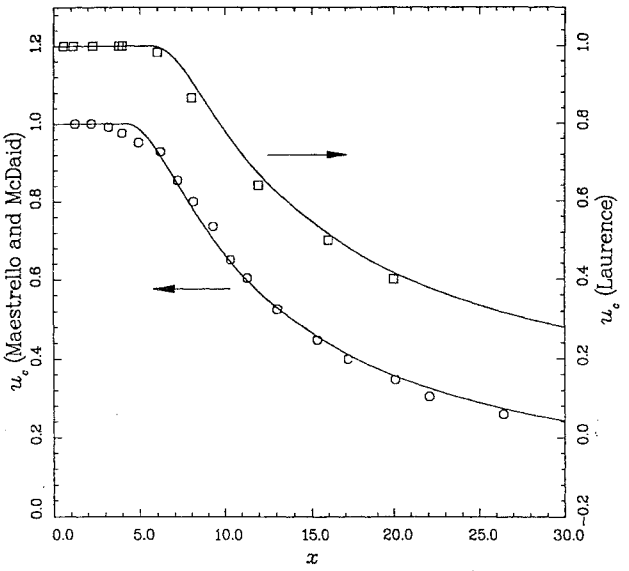

Fig. 5 Comparisons of computed and measured centerline velocity distributions for Maestrello and McDaid's[24] cold, Mach 0.663, axisymmetric jet, ○, and Laurence's[23] cold, Mach 0.7, axisymmetric jet, □.

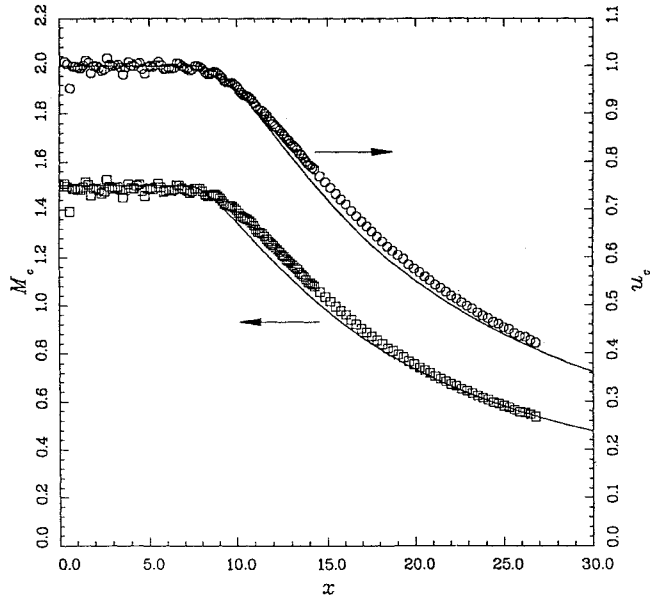

Fig. 6 Comparisons of computed and measured centerline velocity and centerline Mach number distributions for Seiner's[25] T_r/T_n = 1.12, Mach 1.5, axisymmetric jet: ○, measured centerline velocity and □, measured centerline Mach number.

$\partial/\partial x \simeq (1/u_\infty)(\partial/\partial r)$. Therefore, the appropriate dependent variables in this region of the flow (in the sense of a uniformly valid perturbation solution) are $R = Vr$ and $S = p'r$. The appropriate independent variables are x and $\xi = u_\infty r$. Thus Eqs. (22) and (23) may be rewritten as

$$\frac{\partial S}{\partial x} = -\frac{\partial R}{\partial \xi} \tag{24}$$

$$\frac{\partial R}{\partial x} = -\frac{T_\infty}{\gamma M_j^2}\left(\frac{\partial S}{\partial \xi} - u_\infty \frac{S}{\xi}\right) \tag{25}$$

A perturbation solution for small u_∞ in the form

$$\begin{aligned} R(x,\xi) &= R_0(x,\xi) + u_\infty R_1(x,\xi) + u_\infty^2 R_2(x,\xi) + \cdots \\ S(x,\xi) &= S_0(x,\xi) + u_\infty S_1(x,\xi) + u_\infty^2 S_2(x,\xi) + \cdots \end{aligned} \tag{26}$$

can be found by substitution of Eq. (26) into Eqs. (24) and (25).

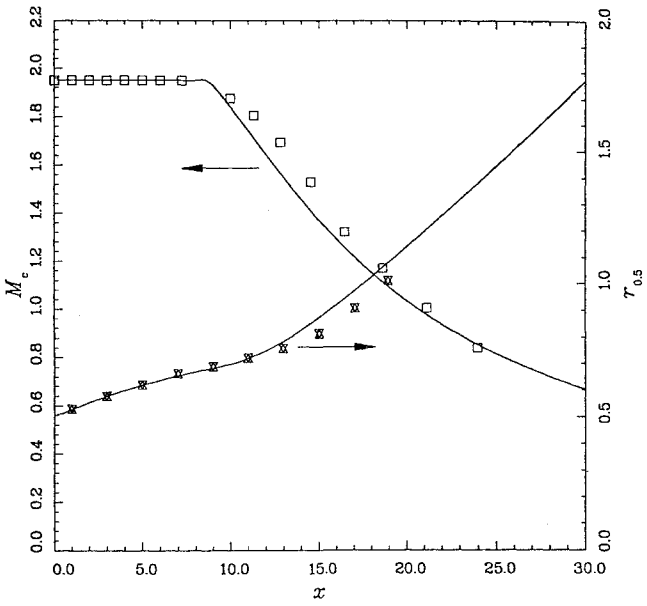

Fig. 7 Comparisons of computed and measured centerline Mach number and half-velocity point distributions for Seiner, et al.'s[26] cold, Mach 2.0, axisymmetric jet: □, measured centerline velocity and ⊠, measured half-velocity point.

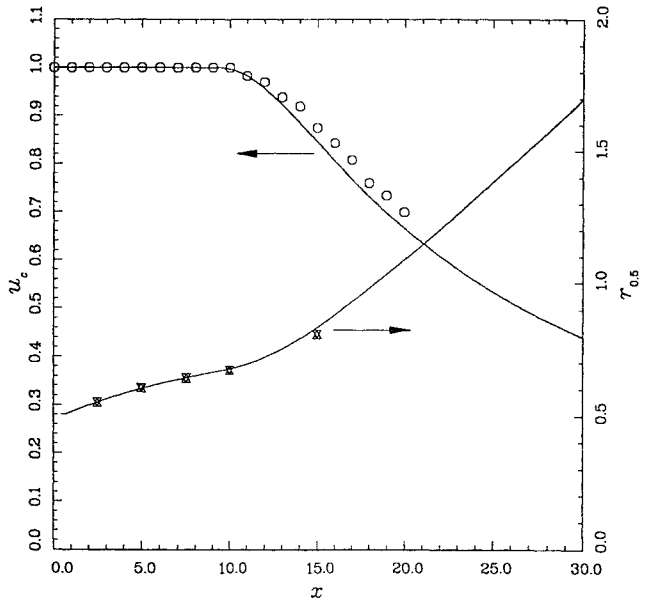

Fig. 8 Comparisons of computed and measured centerline velocity and half-velocity point distributions for Seiner et al.'s[27] T_r/T_n = 1.12, Mach 2.0, axisymmetric jet: ○, measured centerline velocity and ⊠, measured half-velocity point.

Upon partitioning terms according to powers of u_∞, the lowest order outgoing wave solution is found to be

$$\begin{aligned} Vr = R_0(x,\xi) &= F\left(x - \gamma^{\frac{1}{2}} M_j \xi / T_\infty^{\frac{1}{2}}\right) \\ p'r = S_0(x,\xi) &= (\gamma/T_\infty)^{\frac{1}{2}} M_j F\left(x - \gamma^{\frac{1}{2}} M_j \xi / T_\infty^{\frac{1}{2}}\right) \end{aligned} \tag{27}$$

where F is an arbitrary function. On noting that $v = V\cos\phi$ and $w = V\sin\phi$, where r, ϕ, and x are the cylindrical coordinates, the boundary condition for the variables v, w, and p in the region outside the jet flow is obtained by eliminating the unknown function F of Eq. (27) through differentiation. Thus

$$\left(\frac{\gamma}{T_\infty}\right)^{\frac{1}{2}} M_j u_\infty \frac{\partial}{\partial x}\begin{bmatrix} v \\ w \\ p \end{bmatrix} + \frac{\partial}{\partial r}\begin{bmatrix} v \\ w \\ p \end{bmatrix} + \frac{1}{r}\begin{bmatrix} v \\ w \\ p-1 \end{bmatrix} = 0 \tag{28}$$

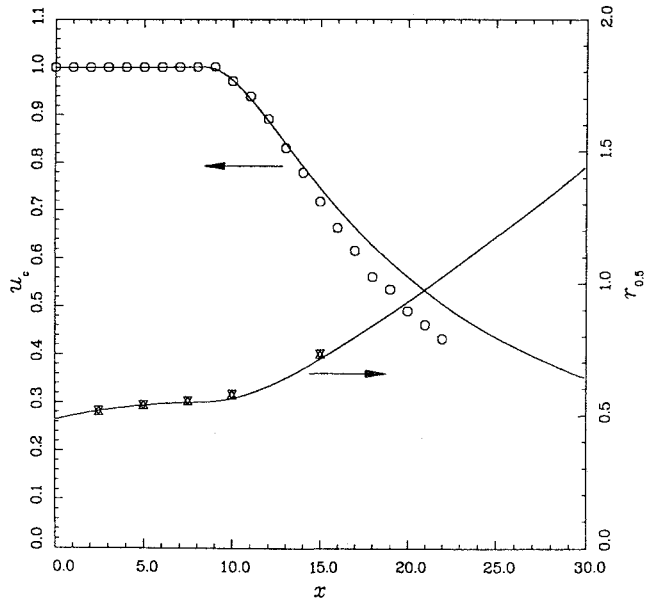

Fig. 9 Comparisons of computed and measured centerline velocity and half-velocity point distributions for Seiner et al.'s[27] T_r/T_n = 2.718, Mach 2.0, axisymmetric jet: ○, measured centerline velocity and ⊠, measured half-velocity point.

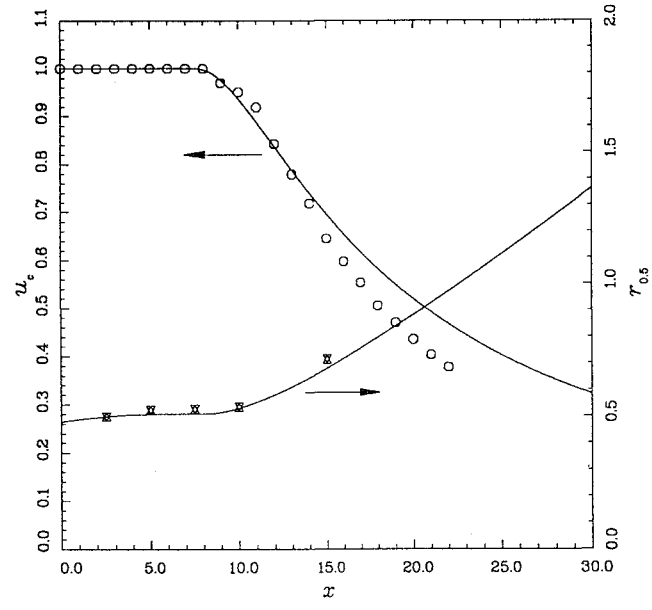

Fig. 10 Comparisons of computed and measured centerline velocity and half-velocity point distributions for Seiner et al.'s[27] T_r/T_n = 4.004 Mach 2.0, axisymmetric jet: ○, measured centerline velocity and ⊠, measured half-velocity point.

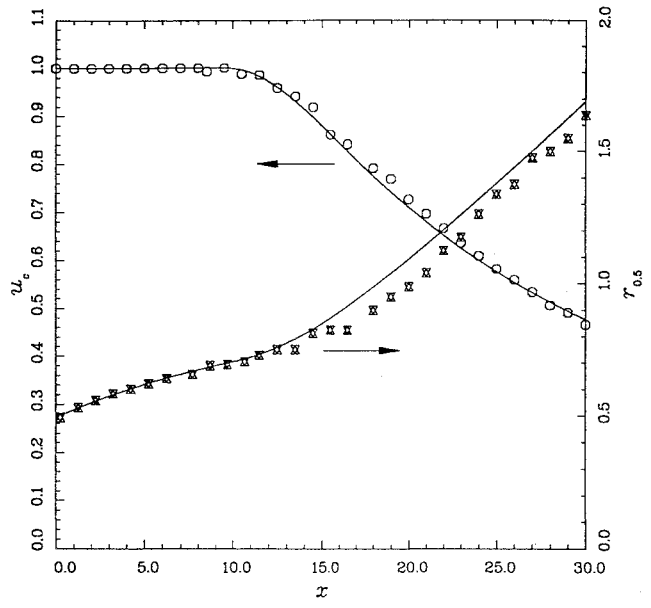

Fig. 11 Comparisons of computed and measured centerline velocity and half-velocity point distributions for Eggers'[28] cold, Mach 2.22, axisymmetric jet: ○, measured centerline velocity; and ⊠, measured half-velocity point.

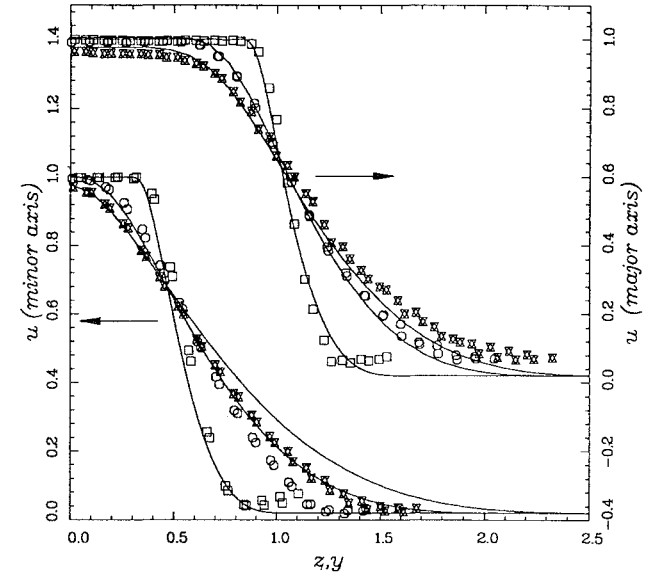

Fig. 12 Comparisons of computed and measured axial velocity profiles in the major and minor axis planes for Schreck et al.'s[22] cold, Mach 0.4, aspect ratio 2, rectangular jet: □, x = 1.778; ○, x = 5.333; and ⊠, x = 7.111.

The boundary conditions for the remaining variables of Eq. (15) are

$$u \to u_\infty, \qquad T \to T_\infty, \qquad K \to 0, \quad \varepsilon_s \to 0 \qquad (29)$$

In the numerical solution of Eq. (15), the spatial derivatives arising from $\partial/\partial r = \cos\phi(\partial/\partial y) + \sin\phi(\partial/\partial z)$ of boundary condition (28) are implemented by using backward difference stencils.[20] Also for axisymmetric, rectangular, and elliptic jets, there are two planes of symmetry. Thus, computation needs to be carried out only in the first quadrant of the y–z plane. On the x–y and x–z planes, symmetry conditions are enforced.

IV. Numerical Results and Comparisons with Experiments

It is our belief that although many of the characteristics of the fine-scale turbulence of most turbulent flows are universally the same, those of the large turbulence structures are not. Because their size is comparable to the characteristic length of the flow, the large turbulence structures are significantly influenced by the local boundary conditions and geometry. These reasonings lead us to suspect the wisdom of using the standard K–ε model coefficients (calibrated using boundary-layer and incompressible two-dimensional mixing layer data) for high-speed turbulent jet flow calculations. Here, instead of the standard coefficients, the following empirically selected values are used in all of the numerical computations:

$$C_\mu = 0.0874, \qquad C_{\varepsilon 1} = 1.40, \qquad C_{\varepsilon 2} = 2.02$$

$$C_{\varepsilon 3} = 0.822, \qquad \gamma\sigma_T = Pr(\text{turbulent Prandtl number}) = 0.422$$

$$\sigma_K = 0.324, \qquad \sigma_\varepsilon = 0.377, \qquad \alpha_1 = 0.518$$

To demonstrate that the K–ε model, together with the Pope and Sarkar corrections and the preceding empirical constants, can

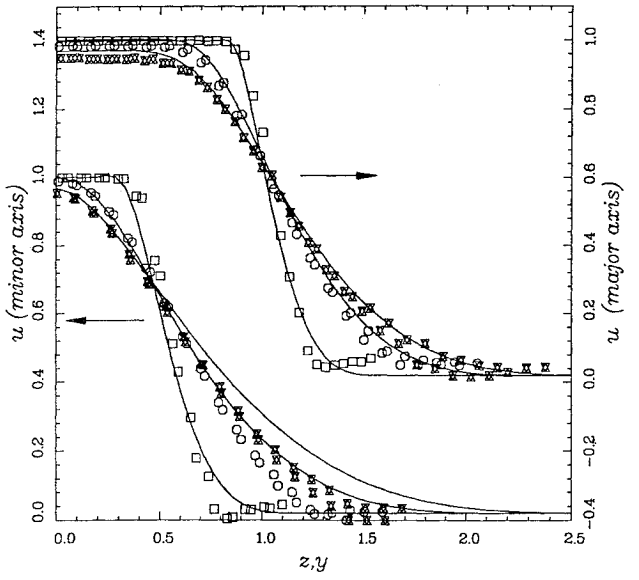

Fig. 13 Comparisons of computed and measured axial velocity profiles in the major and minor axis planes for Schreck et al.'s[22] cold, Mach 0.6, aspect ratio 2, rectangular jet: □, x = 1.778; ○, x = 5.333; and ⊠, x = 7.111.

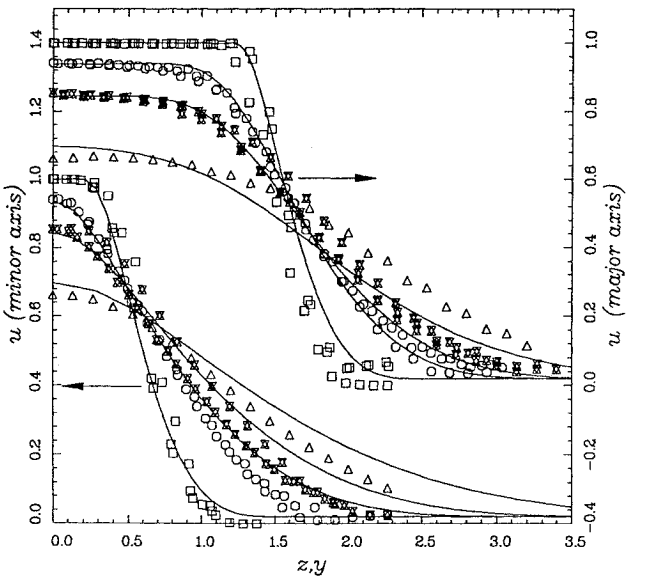

Fig. 15 Comparisons of computed and measured axial velocity profiles in the major and minor axis planes for Schreck et al.'s[22] cold, Mach 0.6, aspect ratio 3, rectangular jet: □, x = 2.667; ○, x = 8.0; ⊠, x = 10.667; and △, x = 16.0.

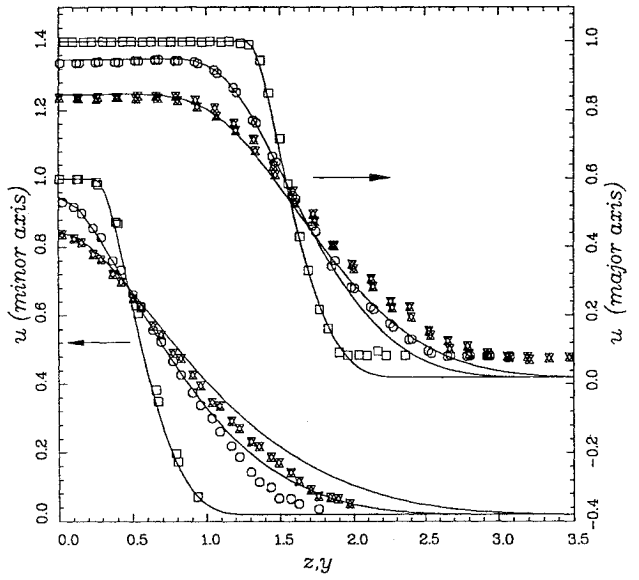

Fig. 14 Comparisons of computed and measured axial velocity profiles in the major and minor axis planes for Schreck et al.'s[22] cold, Mach 0.4, aspect ratio 3, rectangular jet: □, x = 2.667; ○, x = 8.0; and ⊠, x = 10.667.

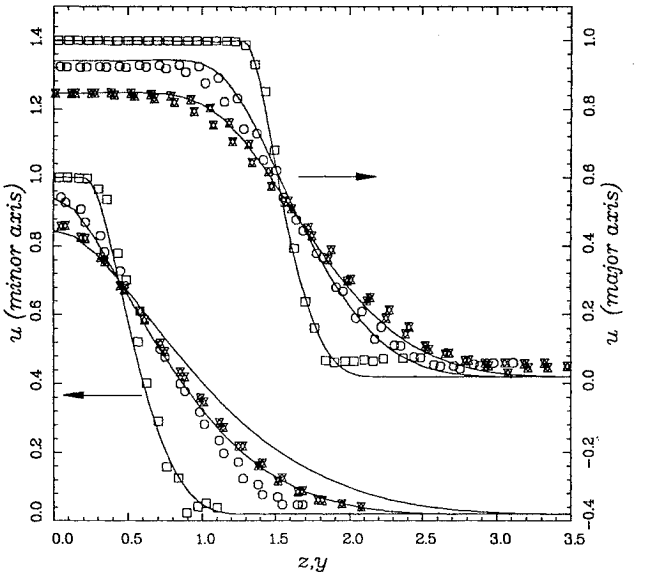

Fig. 16 Comparisons of computed and measured axial velocity profiles in the major and minor axis planes for Schreck et al.'s[22] cold, Mach 0.9, aspect ratio 3, rectangular jet: □, x = 2.667; ○, x = 8.0; and ⊠, x = 10.667.

provide reliable jet mean flow prediction, we have carried out extensive comparisons between numerical results and experimental measurements. In these comparisons, the jet Mach number M_j ranges from 0.4 to 2.2 The jet reservoir temperature to ambient temperature ratio T_r/T_a varies from 1.0 (cold jet) to 4.0. Table 1 lists the source of the 12 sets of axisymmetric jet data for which comparisons have been made. The comparisons are shown in Figs. 1–11. In Figs. 1–4, the computed and measured profiles of the jet axial velocity u as a function of the radial coordinate r are compared. In Figs. 5–11, the axial distributions of the jet centerline velocity u_c, the centerline Mach number M_c, and the half-width of the jet velocity profile $r_{0.5}$ are displayed. As can be seen, there is good agreement in each case. For jet noise prediction purposes, the accuracy of the calculated mean flow is definitely sufficient.

Table 2 lists the source and parameters of the rectangular and elliptic jet data used for comparison. The rectangular jet data are from nozzles of aspect ratio 2 and 3 operating in the subsonic Mach number range. For elliptic jets, only one set of data is available in enough detail in the literature for comparison. In this work, the width of the nozzle in the minor axis plane of the rectangular jets is used as the length scale. The equivalent diameter is used as the length scale for the elliptic jet. Comparisons between the calculated and measured axial velocity distributions in the major and minor axis planes are shown in Figs. 12–17. There are reasonably good agreements. However, they are not as good as for axisymmetric jets. One reason could be that the prescribed initial conditions do not match well with those of the experiment. Also we are informed[29] that the elliptic nozzle used in the experiment has a small dent. This introduces a small asymmetry in the measured velocity profiles even along the major and minor axes. Because of the noncircular geometry of the jets, the mixing rate is nonuniform around the jet perimeter. The numerical results appear to have captured this phenomenon. In the literature, there is almost a complete absence of work on predicting the mean flow of rectangular and elliptic jets. Our finding assures that the K–ε model with appropriate correction terms offers a reliable way for computing this type of flow.

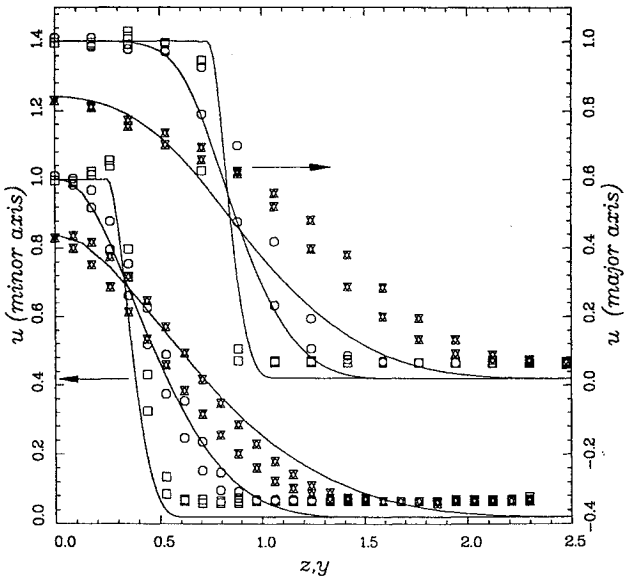

Fig. 17 Comparisons of computed and measured axial velocity profiles in the major and minor axis planes for Seiner's[25] T_r/T_n = 1.12, Mach 1.5, aspect ratio 2, elliptic jet: □, x = 1.265; ○, x = 5.057; and ⊠, x = 10.111.

V. Concluding Remarks

In this work, we have demonstrated that by using a new set of empirical constants, the K–ε model, together with the Pope and Sarkar corrections, can provide accurate jet mean flow predictions over the Mach number range of 0.4–2.0 and jet total temperature to ambient temperature ratio of 1.0–4.0. This applies to axisymmetric as well as nonaxisymmetric jets.

It was stated earlier that the computed results of the parabolized equations are not too sensitive to initial conditions prescribed at the nozzle exit. This is generally true. But a reasonably good set of initial conditions is still needed if an accurate prediction is to be obtained. The fact that the solution does possess some dependence on the initial condition does not reflect a deficiency of the method but rather the actual variability in high Reynolds number jet flows. The jet Mach numbers of Refs. 24 and 23 are nearly the same. The former is 0.663 and the latter is 0.7. However, the jet of Ref. 24 issued from a long pipe nozzle so that the boundary layer at the nozzle was quite thick. As a result, the centerline velocity distributions of the two sets of data as shown in Figs. 5 and 6 are quite different. Thus, the initial conditions used to obtain the velocity distributions are different.

It turns out, in the absence of measurements, that the initial conditions needed for accurate prediction of cold jets are easier to construct than hot jets. Unless the jet is discharged from a very long nozzle, the initial mixing layer thickness of a cold jet is usually very thin. The mixing layer develops very rapidly into a quasi-equilibrium state. For this class of jets, the use of a very thin initial mixing layer will often suffice. In contrast, the Reynolds numbers of hot jets are lower. The initial mixing layers are often in a transition state and only develop into fully turbulent conditions at some distance downstream. Furthermore, the boundary layer at the nozzle exit is often quite thick. Accurate prediction of hot jet mean profiles is, therefore, more difficult. In any case, if the initial profiles are provided, the parabolized code is a reliable prediction tool.

Acknowledgments

This work was supported by NASA Langley Research Grant NAG 1-421. The authors wish to thank S. Schreck and J. M. Seiner for their generous offer of additional experimental data beyond those appearing in Refs. 22 and 25.

References

[1]Tam, C. K. W., and Chen, P., "Turbulent Mixing Noise from Supersonic Jets," *AIAA Journal*, Vol. 32, No. 9, 1994, pp. 1774–1780.

[2]Khavaran, A., Kresja, E. A., and Kim, C. M., "Computation of Supersonic Jet Mixing Noise from an Axisymmetric CD Nozzle Using K–ε Turbulence Model," AIAA Paper 92-0500, Jan. 1992.

[3]Bailly, C., Bechara, W., Lafon, P., and Candel, S., "Jet Noise Predictions Using a K–ε Turbulence Model," AIAA Paper 93-4412, Oct. 1993.

[4]Speziale, C. G., "Analytical Methods for the Development of Reynolds-Stress Closures in Turbulences," *Annual Review of Fluid Mechanics*, Vol. 23, 1991, pp. 107–157.

[5]Hanjalic, K., and Launder, B. E., "A Reynolds Stress Model of Turbulence and Its Application to Thin Shear Flows," *Journal of Fluid Mechanics*, Vol. 52, April 1972, pp. 609–638.

[6]Launder, B. E., and Spalding, D. B., "The Numerical Computation of Turbulent Flows," *Computer Methods in Applied Mechanics and Engineering*, Vol. 3, 1974, pp. 269–289.

[7]Launder, B. E., Reece, G. J., and Rodi, W., "Progress in the Development of a Reynolds Stress Turbulence Closure," *Journal of Fluid Mechanics*, Vol. 68, April 1975, pp. 537–566.

[8]Hanjalic, K., and Launder, B. E., "Contribution Towards a Reynolds Stress Closure for Low Reynolds Number Turbulence," *Journal of Fluid Mechanics*, Vol. 74, April 1976, pp. 593–610.

[9]Pope, S. B., "An Explanation of the Turbulent Round-Jet/Plane-Jet Anomaly," *AIAA Journal*, Vol. 16, No. 3, 1978, pp. 279–281.

[10]Dash, S. M., Sinha, N., and York, B. J., "The Critical Role of Turbulence Modeling in the Prediction of Supersonic Jet Structure for Acoustic Applications," DGLR/AIAA 14th Aeroacoustics Conf., DGLR/AIAA Paper 92-02-106, May 1992.

[11]Dash, S. M., Kenzakowski, D., Lee, R., and Seiner, J. M., "Recent Advances in Jet Flow Simulation: Part 1 Steady Flows," AIAA Paper 93-4390, Oct. 1993.

[12]Bogdanoff, D. W., "Compressibility Effects in Turbulent Shear Layers," *AIAA Journal*, Vol. 21, No. 6, 1983, pp. 926, 927.

[13]Chinzei, N., Masua, G., Komuro, T., Murakami, A., and Kudou, K., "Spreading of Two Stream Supersonic Turbulent Mixing Layers," *Physics of Fluids*, Vol. 29, No. 5, 1986, pp. 1345–1347.

[14]Papamoschou, D., and Roshko, A., "The Compressible Turbulent Shear Layer: An Experimental Study," *Journal of Fluid Mechanics*, Vol. 197, Dec. 1988, pp. 453–477.

[15]Sarkar, S., Erlebacher, G., Hussaini, M. Y., and Kreiss, H. O., "The Analysis and Modeling of Dilatational Terms in Compressible Turbulence," Inst. for Computer Applications in Science and Engineering, NASA Langley Research Center, ICASE Rept. 89-79, Hampton, VA, 1989.

[16]Sarkar, S., and Lakshmanan, B., "Application of a Reynolds Stress Turbulence Model to the Compressible Shear Layer," *AIAA Journal*, Vol. 29, No. 5, 1991, pp. 743–749.

[17]Rubin, S. G., and Tannehill, J. C., "Parabolized/Reduced Navier–Stokes Computational Techniques," *Annual Review of Fluid Mechanics*, Vol. 24, 1992, pp. 117–144.

[18]Thies, A. T., "Computation of Axisymmetric and Nonaxisymmetric Jet Flows and Instability Waves," Ph.D. Thesis, Dept. of Mathematics, Florida State Univ., Tallahassee, FL, 1995.

[19]Tam, C. K. W., and Webb, J. C., "Dispersion-Relation-Preserving Finite Difference Schemes for Computational Acoustics," *Journal of Computational Physics*, Vol. 107, 1993, pp. 262–281.

[20]Tam, C. K. W., "Computational Aeroacoustics: Issues and Methods," *AIAA Journal*, Vol. 33, No. 10, 1995, pp. 1788–1796.

[21]Tam, C. K. W., Webb, J. C., and Dong, Z., "A Study of the Short Wave Components in Computational Acoustics," *Journal of Computational Acoustics*, Vol. 1, March 1993, pp. 1–30.

[22]Schreck, S., Ho, C. M., and Sarmiento, R. S., "Noise Radiated from Axisymmetric and Asymmetric Jets," DGLR/AIAA 14th Aeroacoustics Conf., DGLR/AIAA Paper 92-02-044, May 1992.

[23]Laurence, J. C., "Intensity, Scale and Spectra of Turbulence in Mixing Regions of Free Subsonic Jets," NASA Rept. 1292, 1956.

[24]Maestrello, L., and McDaid, E., "Acoustic Characteristics of a High-Subsonic Jet," *AIAA Journal*, Vol. 9, No. 6, 1971, pp. 1058–1066.

[25]Seiner, J. M., "Fluid Dynamics and Noise Emission Associated with Supersonic Jets," *Studies in Turbulence*, edited by T. B. Gatski, S. Sarkar, and G. Speziale, Springer–Verlag, New York, 1992, pp. 297–323.

[26]Seiner, J. M., McLaughlin, D. K., and Liu, C. H., "Supersonic Jet Noise Generated by Large-Scale Instabilities," NASA TP 2072, Sept. 1982.

[27]Seiner, J. M., Ponton, M. K., Jansen, B. J., and Lagen, N. T., "The Effects of Temperature on Supersonic Jet Noise Emission," DGLR/AIAA 14th Aeroacoustics Conf., DGLR/AIAA Paper 92-02-046, May 1992.

[28]Eggers, J. M., "Velocity Profiles and Eddy Viscosity Distributions Downstream of a Mach 2.22 Nozzle Exhausting to Quiescent Air," NASA TN-3601, Sept. 1966.

[29]Seiner, J. M., private communication.